# Mode resonance and wavelength-halving instability in the Taylor-Dean system

Innocent Mutabazi
*Groupe d'Energétique et de Mécanique, Université du Havre, Boîte Postale 540, F-76058, Le Havre, France*

C. David Andereck
*Department of Physics, The Ohio State University, 174 West 18th Avenue, Columbus, Ohio 43210*
(Received 11 August 1994)

We investigate experimentally the higher modes of the Dean vortex flow in the regime of resonant fundamental and second harmonic modes in the Taylor-Dean system. An unusual transition sequence to spatiotemporal chaos is observed: stationary Dean vortex flow gives way to a drift instability followed by a wavelength-halving instability. The resulting small rolls are modulated in space and time, and they form a roll packet that preserves the initial spatial period. The linear and nonlinear stability analysis of the flow shows that the interaction of resonant modes leads to some of the observed results. The wavelength-halving instability may also be attributed to a second harmonic generation.

PACS number(s): 47.20.−k, 47.52.+j, 47.32.−y

## I. INTRODUCTION

Recently, one-dimensional extended systems far from equilibrium exhibiting bifurcations to tilted, drifting patterns have attracted much attention. This type of bifurcation has been observed in the Taylor-Couette system [1], in the Taylor-Dean system [2–4], in directional solidification of liquid crystals [5], in lamellar eutectic growth [6], and in directional viscous fingering [7]. These observations have provided the sufficient basic ingredient for several attempts at theoretical modeling [8–13]. This special attention has been motivated by the leading role played by the natural breaking of symmetries in these systems, which manifests itself in the occurrence of a frequency in the pattern, in roll pattern drifting, or in the occurrence of localized traveling pulses or spatiotemporal defects. Recent developments in the nonlinear Ginzburg-Landau theory for dissipative systems have provided insight into some of the experimental results such as the existence of the localized pulselike structures in the cellular pattern, and the dynamics of defects [9,14]. In these theoretical studies, particular attention was drawn to the mechanism of the second harmonic interaction with the fundamental mode. Although the importance of the interaction of the fundamental with the second harmonic modes in nonlinear optics has been appreciated for some years [15,16], it was not until recently that the application to dissipative dynamical systems has been attempted. Such a model was developed by Malomed and Tribelsky [17] in the context of the Kuramoto-Sivashinsky equation and has been applied by Fauve, Douady, and Thual [11] to explain the drift instability observed in several of the experiments.

Fundamental and second harmonic interactions can have additional consequences. For example, spatial period doubling has been observed in directional solidification when the interface is driven rapidly above the drift threshold and then rapidly driven back to a cellular regime [5]. When the Taylor-Couette system with slightly counterrotating cylinders is driven far away from the linearly stable state, patterns exhibiting spatial period doubling were found by Wiener and McAlister [18], in agreement with numerical calculations [19]. These cases of spatial second harmonic generation are a consequence of a "forced" wavelength selection process. However, there exist many hydrodynamic systems in which linear stability analysis predicts the existence of resonant fundamental and second harmonic modes, but with either limited or no experimental evidence so far: the hydromagnetic Taylor-Couette instability [20], the flow between two horizontal concentric cylinders with a transverse pressure gradient [21], double layer thermal convection [22], and a slight variant, thermal convection in superposed layers of immiscible fluids [23,24]. The mathematical investigation of the interaction of resonant spatial modes, and of modes with different spatial scales, has been addressed in [22,25].

This paper reports recent experimental results from a nearly one-dimensional pattern-forming system in which the second spatial harmonic of a pattern arises naturally (without a "forcing procedure") when the system is driven continuously from the base flow state to various cellular patterns. The system consists of two horizontal coaxial cylinders with a partially filled gap, usually referred to as the *Taylor-Dean system* [3,4]. Since the two cylinders may rotate independently, the flow evolution is described in a two parameter space $(R_o, R_i)$ defined below. In contrast with the Taylor-Couette system [26], the partial filling of the gap produces two free surfaces, which break the rotational symmetry of the Couette flow and may lead to quite different flow states. The rotation of the cylinders drives the fluid toward the free surfaces, and to reverse it, a pressure gradient along the azimuthal direction is created. Far away from the free surfaces, the flow velocity profile is a combination of Couette flow due to the cylinder rotation and Poiseuille flow due to the azimuthal pressure gradient. The streamline curvature induces a radial stratification of the fluid particle momen-

 

tum. Rayleigh's stability criterion [3,26] predicts, in the case of negative momentum stratification, that centrifugal instabilities may arise, producing longitudinal rolls periodically spaced in the spanwise (axial) direction. Detailed linear and nonlinear stability analysis of the flow shows that, depending on the angular velocities of the cylinders, the destabilization of the different potentially unstable zones gives rise to several different modes. Both stationary and traveling roll patterns may arise with different wave numbers, the ratio between them varying from 1 to 2.5 [2,27]. Thus, the Taylor-Dean system realizes a quasi-one-dimensional extended system with competing instabilities of various wavelengths. The interaction of these modes should lead to different patterns than what has been observed in other experimental configurations.

The aim of this work is to describe in detail the observations previously reported [30] and to put them in the context of recent theoretical developments. The paper is organized as follows: Sec. II describes the experimental setup and procedure. In Sec. III, we present the experimental results and Sec. IV contains results from the linear stability analysis. The model of second harmonic interaction in the generation of drift instabilities is presented in Sec. V. The last section consists of concluding remarks.

## II. EXPERIMENTAL SETUP

The experimental system essentially consists of two horizontal coaxial cylinders [Fig. 1(a)] mounted in such a way that each can rotate independently of the other. The inner cylinder, made of black Delrin plastic with radius $a=4.49$ cm, rotates at angular velocity $\Omega_i$, and the outer, with radius $b=5.08$ cm, is made of precision ground and polished Duran glass and, in this experiment, rotates in the same direction as the inner at angular velocity $\Omega_o$. The gap between the cylinders is $d=b-a=0.59$ cm, and the radius ratio $\eta=a/b=0.88$. Teflon rings are attached to the inner surface of the outer cylinder a distance $L=53.40$ cm apart, giving an aspect ratio $\Gamma=L/d=90$, large enough to realize a quasi-one-dimensional extended system. The cylinders are driven by Compumotor stepper motors which are precise to $0.25\times10^{-3}$ Hz. The working fluid is water with 1% Kalliroscope AQ1000 added for visualization. Its kinematic viscosity is $\nu=0.98\times10^{-2}$ cm$^2$/sec at the temperature $T=21$ °C, the average temperature in our controlled laboratory environment.

We define the flow control parameters to be the Reynolds numbers relative to the inner and outer cylinders, respectively, $R_i=\Omega_i ad/\nu$, $R_o=\Omega_o bd/\nu$. In this experiment, the outer cylinder was kept rotating at a fixed angular velocity, and we varied slowly (quasistatically) the inner cylinder angular velocity from the base flow state through successive bifurcations. In order to achieve quasistatic conditions and thus avoid spurious hysteresis [31], we have chosen the ramping rate (experimental variation of the inner cylinder Reynolds number) $r=dR_i/dt^*\leq 3$ where $t^*=t/\Gamma$. The Reynolds numbers are measured to within $\pm2\%$.

Flow frequencies are measured from the power spectra of single-point time series obtained with laser light that is reflected off the Kalliroscope flakes onto a photodiode detector. Spatial dependence data are obtained using a 28–35 mm variable focal length lens to form an image of the visualized flow on a 1024-pixel charge-coupled device linear array interfaced through a computer automated measurement and control (CAMAC) system to a PDP-11/73 computer. The line of 1024 pixels is oriented parallel to the cylinder axis, and about 3 cm below a free surface. (This is far enough from the surface to be effectively in the bulk flow region.) The output consists of intensity maxima and minima which correspond to the centers and boundaries of the rolls. Space-time diagrams are then produced by displaying intensity versus axial position plots at regular time intervals ($\Delta t=0.07$ or 0.14 sec). An analysis of these plots yields the roll size and the

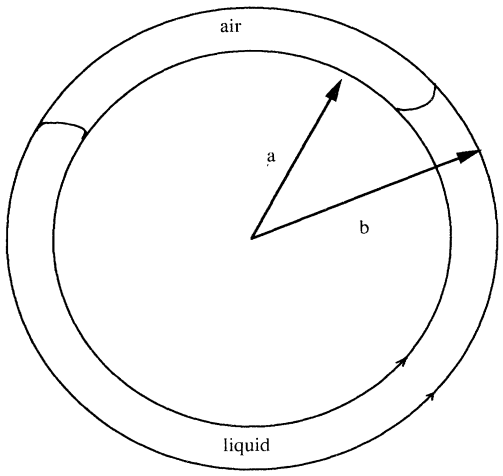


(a)

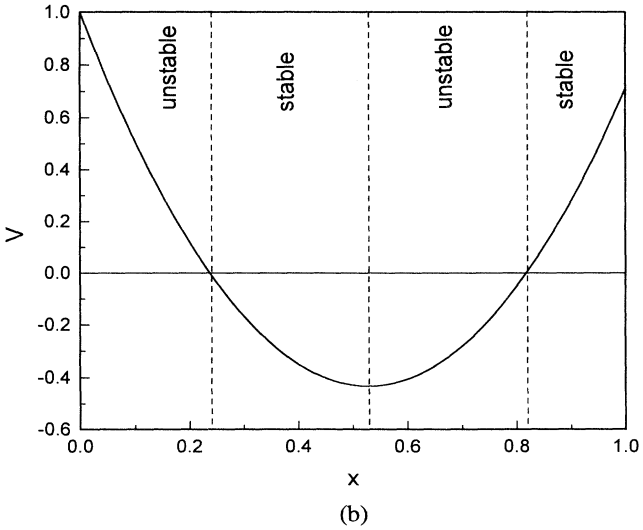


(b)

FIG. 1. (a) Schematic representation of the experimental geometry of the Taylor-Dean system. (b) Base velocity profile for $\mu=0.714$ far from the free surfaces: potentially unstable and stable zones after the Rayleigh stability criterion.

dynamics of the pattern in time and in space. The spatial periodicity of the flow pattern is characterized by the nondimensional wave number $q=2\pi d/\lambda$, and its time dependence is characterized by the propagation velocity $v$ or the roll frequency $f$.

## III. RESULTS

The main experimental results to be described in this section are represented in the parameter space $(R_o,R_i)$ shown in Fig. 2(a), where $R_o \in [205,250]$. The critical values of the control parameter $R_i$ for the first and second transitions depend sensitively on the outer cylinder Reynolds number $R_o$. Figure 2(b) shows the schematic transition diagram for the particular value of $R_o=213$.

### A. Transition from stationary to traveling rolls

The first instability from the laminar base flow gives rise to stationary axisymmetric Dean rolls aligned along the circumferential direction [Fig. 3(a)]. Within our experimental error of 2% in $R_i$ and the step size of 0.2%, this is found to be a supercritical bifurcation. This roll pattern possesses also the reflection symmetry $(z\rightarrow -z)$, where $z$ is the axis of the system. The roll wave number

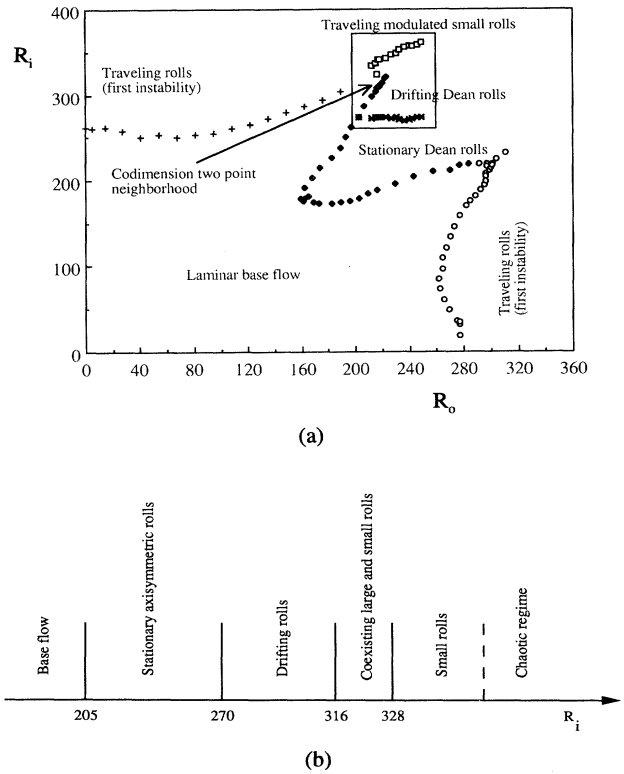


FIG. 2. (a) Region of interest in the right part of the experimental parameter space $(R_o,R_i)$ in the neighborhood of the codimension two point. The transitions to higher instabilities in other parts of the diagram are different from those described here. A complete parameter space of states is given in [29]. (b) Schematic picture of the transitions for $R_o=213$.

is $q=3.40\pm0.05$. The second instability occurs via a supercritical bifurcation (again there is no hysteresis within our experimental limits) in which the rolls begin to travel along the axial direction [Fig. 3(b)]. The propagation velocity of the rolls at the onset is of order $10^{-2}$ cm/sec $=0.6\nu/d$. This behavior is often called a *drift instability* [11]. As the rolls begin to drift, they also begin to incline in the propagation direction. Therefore the drift instability is a result of the spontaneous breaking of the pattern reflection symmetry. Figure 4 shows the drift frequency measured from the power spectrum of the intensity of light reflected off the roll pattern. The traveling rolls have a wavelength slightly larger than that of the stationary rolls.

Just above onset of the drift instability, for all values of $R_o$ for which drifting is observed, the traveling roll pattern is subject to a phase instability that results in roll collisions and roll generation. The roll generation adds a roll to the pattern (roll creation) and the collision of two rolls removes a roll from the pattern (roll annihilation). For each experimental run, these roll creation and annihilation events occur at different axial positions and have a time period approximately equal to the roll drift period [a typical example is shown in Fig. 5(a) for $R_o$ different from that of Fig. 3; qualitatively the behavior is similar for different $R_o$, although the details may change]. Each roll creation or annihilation process has a finite lifetime corresponding to the accumulation or release of "energy" by the pattern. The points in the space-time diagram where collision and generation take place are called *spatiotemporal* defects or grain boundaries [9,32]. We have observed that the total number of these defects, which depend on the control parameter $R_i$ and on the experimental ramping rate, is an odd number: 1,3,5..., possibly a reflection of the presence of end boundaries.

A further increase of $R_i$ leads to either the extinction of the pattern for $205<R_o<213$ (Fig. 2) or to pattern weakening detected visually by a loss of contrast and quantitatively by the measured decrease of the drift frequency $f_d$ for $R_o>213$ [Fig. 5(b)]. This is qualitatively consistent with the prediction of the drift instability model, to be presented in Sec. V, that the drift frequency is proportional to the roll amplitude near the onset of the drift instability. Quantitative comparison was not possible since the relationship between the observed contrast variations and the actual amplitude of the mode is not known.

### B. Wavelength-halving instability

Near $R_o=213$, there is neither roll weakening nor roll extinction, but the transition occurs for $R_i=315$ to a pattern with large rolls and small rolls occupying different regions along the system axis. A large roll propagates and splits, at an axial position which depends on $R_i$, into two rolls of different sizes [Fig. 3(c)] which propagate in the same direction and with approximately the same drift velocity as the parent roll. Such states are observed for $R_o=213$ in a finite range of the control parameter values $R_i \in [315,330]$. The *codimension two points* in the pa-

rameter space $(R_o, R_i)$ are where the large and small rolls coexist. The range of the values of $R_i$ in which this coexistence is observed decreases as $R_o$ increases. Therefore there exists a whole region of codimension two points in the parameter space $(R_o, R_i)$ [Fig. 2(a)]. The generally observed case is that where large rolls occupy a part (e.g., the left part) of the flow pattern and the small rolls occupy the remainder (right); however, states with small rolls sandwiched between two regions of large rolls have also been observed. The occurrence of small rolls reduces the domain of large rolls until their disappearance from the pattern when the control parameter is slightly increased. The points in the space-time diagram where large rolls split into small rolls form a line which could be called a *spatiotemporal wall.* The average wall position in the space-time diagram depends on the control parameter value $R_i$, and, for a fixed value, the spatiotemporal wall position fluctuates in space and time [Fig. 3(c)] in a zone of approximately a large roll size in width.

For $R_o \geq 213$, for a small increase of $R_i$, the weak rolls give rise to small rolls which in turn tend to displace the large weak rolls. The small rolls are periodically modulated in space and time (their intensity increases and then decreases as they propagate) and they behave like a two-roll packet (drifting at the same velocity) in which the rolls exchange "energy" [Fig. 3(d)]. We should mention also that in the small rolls region, we have observed, localized in space and time, remanent rolls from the large roll pattern. For $R_o < 213$, a further increase of $R_i$ leads to the occurrence, in the patternless flow, of traveling rolls, the size of which is about half that of the former, extinct rolls.

Figure 6 shows a Fourier spectrum of the spatial distribution of light intensity reflected from the roll pattern when the second harmonic peak becomes comparable in power with the fundamental. In all cases, the Fourier spectra show that the frequencies and the mean wave numbers of the small roll and large, superseded, roll pattern states are in a ratio close to 2:1; the differences $\Delta f = f_h - 2f_d \sim 0.01$ and $\Delta q = q_2 - 2q_1 \sim 0.20$ are due to spatiotemporal modulations of the small rolls and other temporal and spatial phase gradient related instabilities.

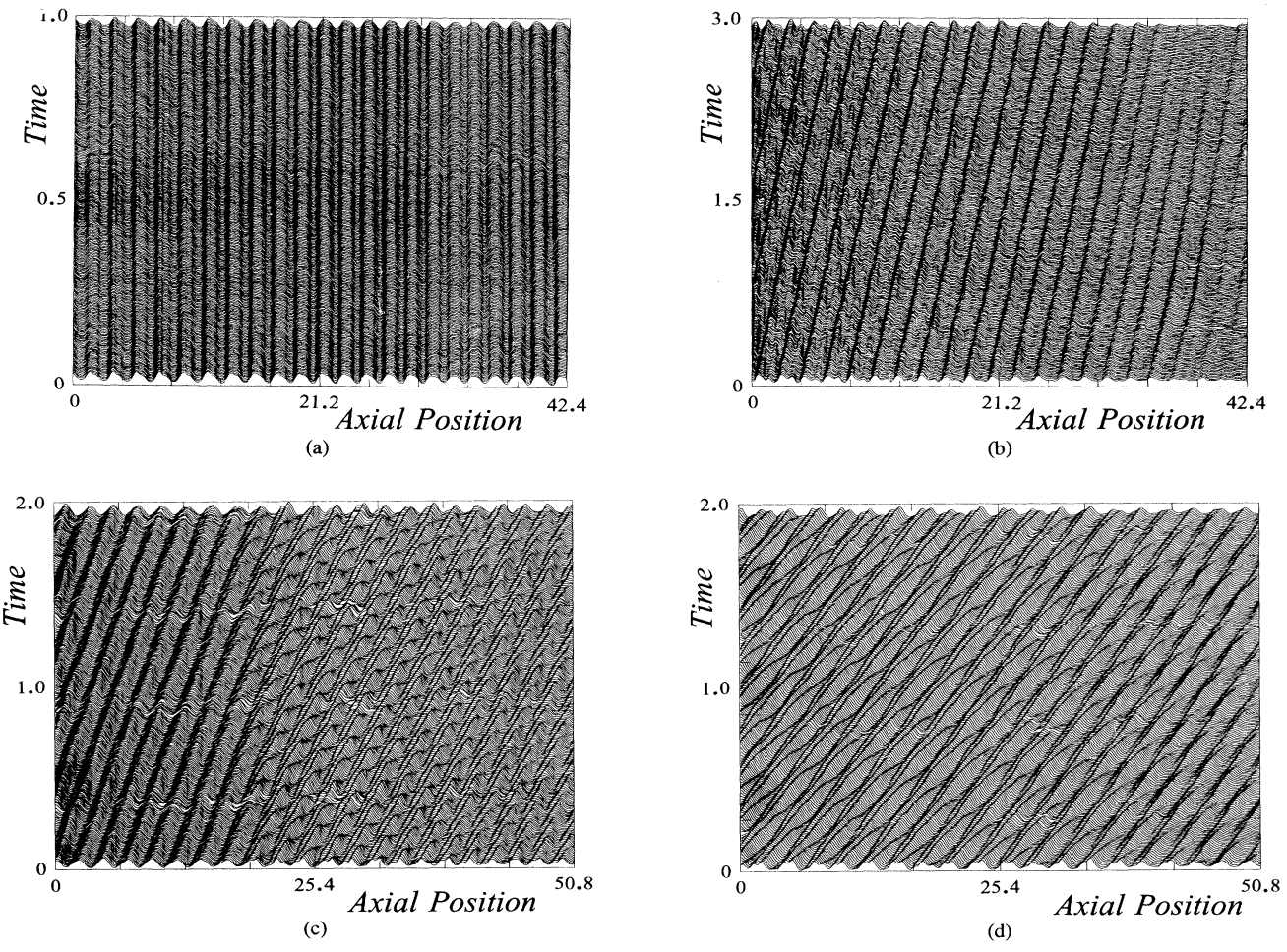


FIG. 3. Space-time diagrams of different states of the roll pattern for $R_o = 213$: (a) stationary Dean rolls ($R_i = 214$), (b) drifting rolls ($R_i = 299$), (c) roll pattern with two coexisting wavelength states separated by a wall ($R_i = 318$) (each large roll splits into two rolls of different sizes which propagate in the same direction forming a two-roll packet), (d) pure state of small modulated rolls ($R_i = 331$).

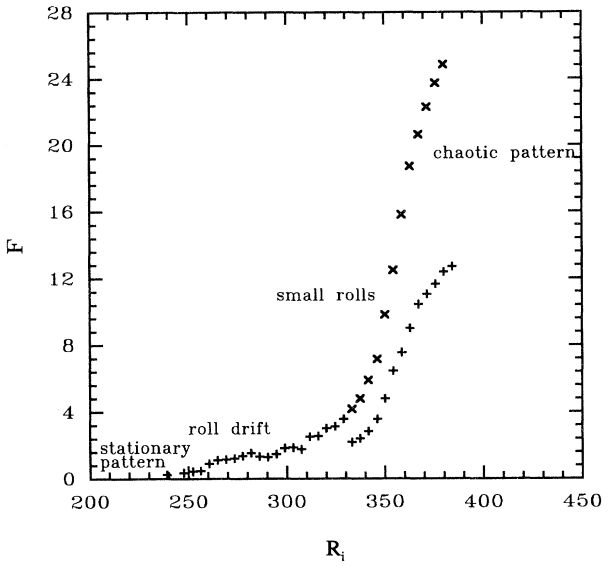


FIG. 4. Dimensionless drift frequency (proportional to the roll drift velocity) as a function of the control parameter $R_i$ for fixed $R_o=242$. Stationary rolls are observed for $R_i \in [202,238]$, the drift instability occurs at $R_i=239$, and the second harmonic peak also becomes prominent at $R_i \simeq 330$. The small rolls occur approximately at $R_i=340$. The small rolls drift at approximately the same velocity as the large rolls. For this value of $R_o$, the coexistence between large and small rolls has not been observed. For $R_i > 370$, the peaks of the fundamental and second harmonic broaden, so we consider the pattern to be chaotic. (+) correspond to the fundamental mode peak and (×) to the second harmonic mode peak.

Since the second frequency $f_h$ is almost twice the former drift frequency ($f_h \simeq 2f_d$) and the small rolls are about half the size of the former rolls as seen from the space-time plot (Figs. 3 and 5), this transition may be called a *wavelength-halving instability*

A further increase of the control parameter leads to a roll pattern with only small modulated rolls exhibiting an apparently chaotic behavior [Fig. 5(c)] in which standing waves can also be detected.

## IV. LINEAR STABILITY THEORY

We have performed the linear stability analysis of the Taylor-Dean system [27,29] and now summarize the results that pertain to the present experiment. In the small gap approximation ($d/a \ll 1$), the base flow in the core region of the Taylor-Dean system (i.e., far away from the free surfaces) is given by

$$V(x)=3(1+\mu)x^2-2(2+\mu)x+1 , \quad (1)$$

where $x=(r-a)/d$ is the nondimensional radial coordinate and $\mu=\Omega_o/\Omega_i$ is the rotation velocity ratio of the cylinders. Such a parabolic velocity profile allows for a simple physical interpretation of the instability mechanisms. In fact, on the basis of Rayleigh's stability criterion, such a profile has, for $\mu > 0$, two potentially unstable layers alternating with stable layers [Fig. 1(b)]. The inner unstable layer is in the Couette part of the profile and it must therefore give rise to the Taylor-Couette instability, while the outer unstable layer is in the Poiseuille part of the velocity profile and must likewise give rise to the Dean instability. The perturbation $\mathbf{v}'$ to the basic flow (1) is expanded into normal modes $\mathbf{v}'=(u,v,w)\exp(st+iqz+ipy)$ where $q$ and $p$ are the real axial and azimuthal wave numbers and $s$ is the complex amplification rate of the perturbations. The linear stability analysis of this parabolic velocity profile has shown that for $\mu > 0.584$, the critical modes are stationary and axisymmetric [27], i.e., $s=p=0$. Elimination of the pressure field $p$ and of the axial velocity component $w$ from the linearized Navier-Stokes equations gives the following system of equations for the stationary perturbative velocity field:

$$(D^2-q^2)^2u-2q^2\mathrm{Ta}V(x)v=0 , \quad (2)$$

$$(D^2-q^2)v-\mathrm{Ta}DVu=0 , \quad (3)$$

together with the homogeneous boundary conditions

$$u=Du=v=0 \quad \text{at } x=0,\ x=1 , \quad (4)$$

where the parameter $\mathrm{Ta}=(\Omega_i ad/\nu)(d/a)^{1/2}$ is the Taylor number [28]. These equations have been solved numerically and the topology of the marginal stability curves has been discussed thoroughly in [27] for corotating cylinders $\mu > 0$. The finite gap case has been investigated recently in [33] for $\mu \in [-5,5]$, and for the range of $\mu$ under consideration there is no significant difference in the critical states of the first instability. We consider $\mu \in [0.6,0.8]$ which is the range of values of $(R_o,R_i)$ considered in this experiment [34]. In that range, the eigenvalue problem defined by Eqs. (2) and (3) and the homogeneous boundary conditions (4) has two stationary marginal curves [Fig. 7(a)] $\mathrm{Ta}=\mathrm{Ta}(q)$: for the particular value of $\mu=0.714$, the lower stability curve has a minimum at $q_1=4.34$, $\mathrm{Ta}_1=113.59$, and corresponds to the Dean instability as its eigenfunction is centered in the Poiseuille unstable zone of the base flow. The upper sta-

TABLE I. Critical parameters of the Dean ($q_1$,$\mathrm{Ta}_1$) and Taylor ($q_2$,$\mathrm{Ta}_2$) modes, together with the ratios $n=q_2/q_1$ and $r=\mathrm{Ta}_2/\mathrm{Ta}_1$.

| $\mu$ | $q_1$ | $\mathrm{Ta}_1$ | $q_2$ | $\mathrm{Ta}_2$ | $n$ | $r$ |
|---|---|---|---|---|---|---|
| 0.650 | 4.48 | 121.26 | 8.44 | 221.59 | 1.88 | 1.83 |
| 0.700 | 4.37 | 115.18 | 8.63 | 229.12 | 1.97 | 1.99 |
| 0.705 | 4.36 | 114.61 | 8.64 | 229.86 | 1.98 | 2.01 |
| 0.710 | 4.35 | 114.04 | 8.66 | 230.61 | 1.99 | 2.02 |
| 0.714 | 4.34 | 113.59 | 8.68 | 231.21 | 2.00 | 2.04 |
| 0.720 | 4.33 | 112.91 | 8.70 | 232.10 | 2.01 | 2.06 |
| 0.730 | 4.30 | 111.81 | 8.74 | 233.60 | 2.03 | 2.09 |
| 0.750 | 4.26 | 109.66 | 8.82 | 236.60 | 2.07 | 2.16 |
| 0.800 | 4.17 | 104.60 | 9.01 | 244.11 | 2.16 | 2.33 |
| 0.850 | 4.08 | 99.94 | 9.20 | 251.64 | 2.25 | 2.53 |
| 0.885 | 4.02 | 96.89 | 9.33 | 256.94 | 2.32 | 2.65 |
| 0.900 | 4.00 | 95.64 | 9.34 | 259.23 | 2.34 | 2.71 |
| 0.950 | 3.92 | 91.65 | 9.57 | 266.86 | 2.44 | 2.91 |
| 1.000 | 3.85 | 87.93 | 9.76 | 274.56 | 2.53 | 3.12 |

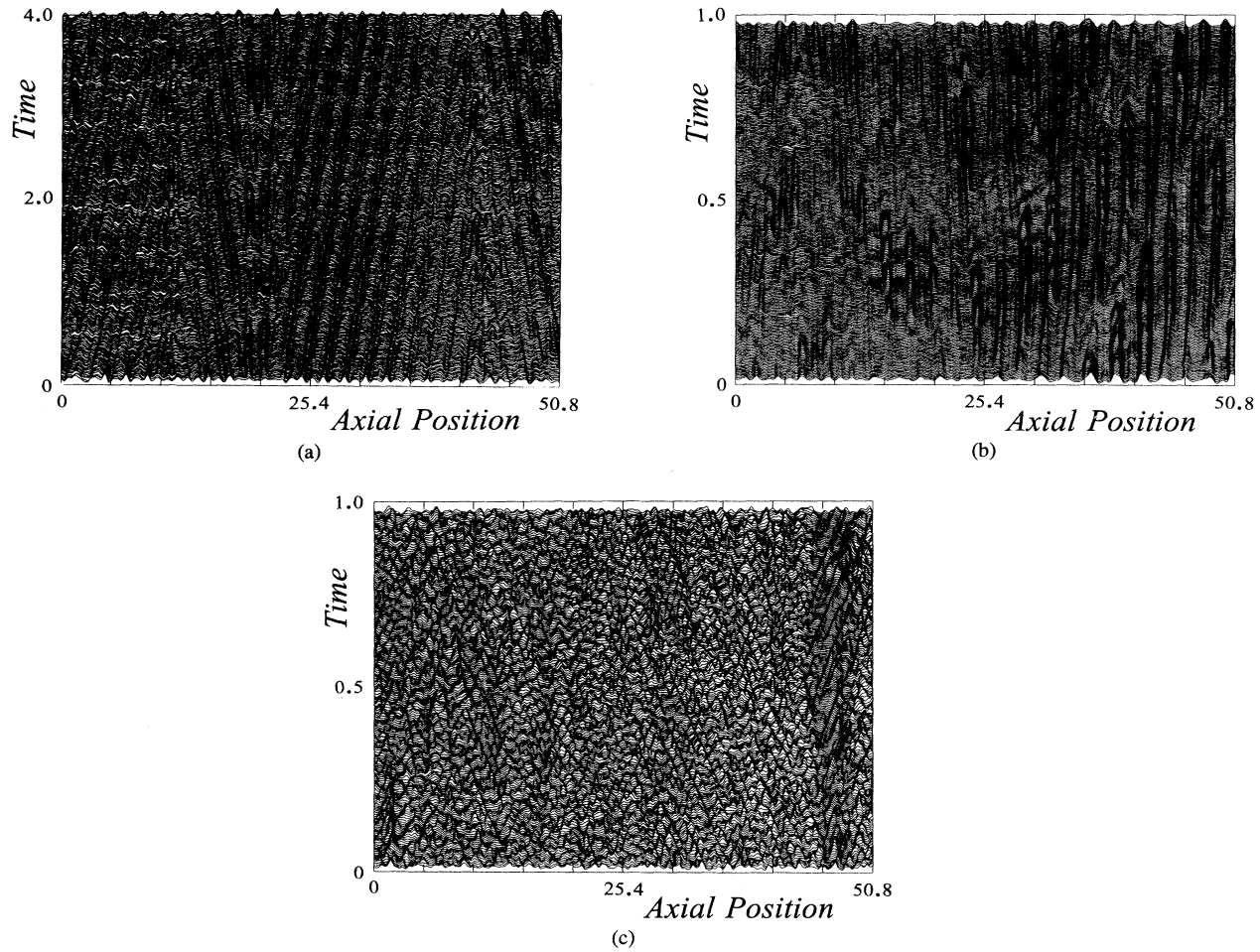


FIG. 5. Space-time diagram of time-dependent states for $R_o=242$: (a) traveling roll pattern with spatiotemporal defects for $R_o=242$, $R_i=282$. In this pattern, representing 60% of the whole flow pattern, there are three positions where spatiotemporal defects occur, $z_1=6.4$ cm$=10.8d$, $z_2=12.2$ cm$=20.5d$, $z_3=25.8$ cm$=43.5d$, where the left end of the pattern is located at 9.7 cm$=16.3d$, away from the origin of this plot. The period between defects at the same position is 28 sec$=0.78d^2/\nu$ for $R_o=242$, $R_i=282$. The whole pattern contains five defects (three sourcelike and two sinklike). In the sourcelike defect, a roll splits into two rolls; in the sinklike defect, two rolls collide to form one roll. (b) Weakening of the roll pattern ($R_i=332$); the roll amplitude changes significantly over time while the external conditions are maintained constant. (c) Chaotic state as a mixture of standing and traveling rolls ($R_i=393$).

bility curve has a minimum at $q_2=8.68$, $\mathrm{Ta}_2=231.21$, and is associated with the Taylor instability as its eigenfunction is centered in the Couette unstable zone of the base flow [Fig. 1(b)] [27]. The second mode (Taylor mode) has a critical wave number $q_2$ of the order of twice that of the fundamental Dean mode $q_1$ over the range of $\mu$ considered (see Table I). For $\mu=0.714$, the Dean mode and the Taylor mode become perfectly resonant ($q_2=2q_1$) and therefore may interact strongly. But mode interaction is a nonlinear phenomenon and therefore it cannot be described by the linear stability analysis. The nonlinear interaction of these Dean and Taylor modes is the subject of the next section.

To complete the linear analysis, it is necessary to study the stability of long-wavelength perturbations, i.e., to determine the Eckhaus stability boundary. The Eckhaus stability curve of the one-dimensional long-wavelength stationary perturbations is given by the equation

$$\mathrm{Ta}(q)=\mathrm{Ta}_1[1+3\xi_0^2(q-q_c)^2] ,$$

where $\xi_0$ is the perturbation correlation length and depends on the rotation ratio $\mu$ [33]. The experimental wave numbers of the large rolls (Dean rolls and drifting rolls) lie in the Eckhaus stable zone while those of the small rolls fall in the Eckhaus unstable zone [Fig. 7(b)]. Thus the small rolls probably correspond to the stable second harmonic mode (Taylor modes) which supercedes the fundamental mode in the Dean mode's Eckhaus unstable zone.

## V. DRIFT INSTABILITY MODEL

The linear stability analysis shows that the Taylor-Dean system exhibits two modes which are spatially reso-

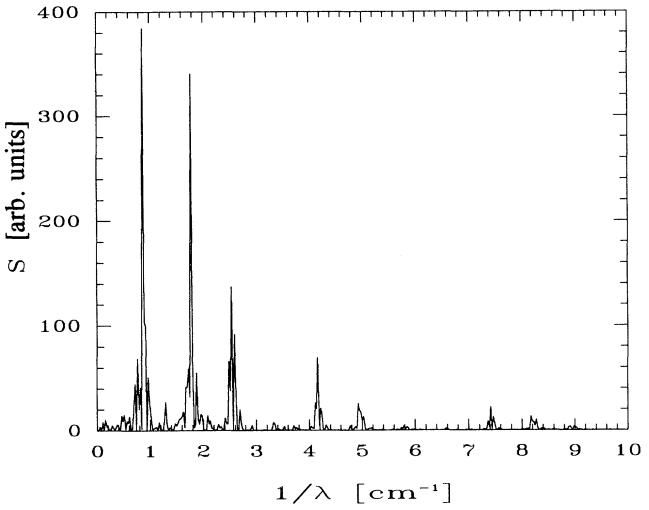


FIG. 6. Fourier spectra of light intensity distribution along the roll pattern for $R_o=213$, $R_i=299$. The large roll pattern is drifting. The first peak corresponds to the wave number $q=3.22$, while the second harmonic peak ($q=6.631$) is also prominent.

nant for $\mu=0.714$: the Dean mode with critical wave number $q_1$ plays the role of the fundamental mode and the Taylor mode with critical wave number $q_2=2q_1$ is the second harmonic mode. Following the general nonlinear analysis of resonant stationary modes [11,22], we show that the interaction of the Dean and Taylor modes may lead to observed features related to the second harmonic interaction. The basic analysis is strictly true for the value $\mu=0.714$, but it can be extended to other values of $\mu$ corresponding to the experimental data $\mu\in[0.65,0.80]$ by taking into account the phase mismatching due to the wave number difference $\Delta q=q_2-2q_1$.

### A. Coupled amplitude equations

The perturbation flow velocity field may be written as follows:

$$\mathbf{v}(t,\mathbf{r})=A(t,z)\mathbf{F}_1e^{iq_1z}+B(t,z)\mathbf{F}_2e^{iq_2z}+\text{c.c.}+\text{h.o.t.}\ , \tag{5}$$

where c.c. stands for complex conjugate and h.o.t. stands for higher order terms, $A(t,z)$ and $B(t,z)$ are slowly varying complex amplitudes corresponding to the Dean and the Taylor modes, respectively, and $\mathbf{F}_1(x)$ and $\mathbf{F}_2(x)$ are their eigenvectors. The amplitude equations for $A$ and $B$ satisfying translational invariance are

$$\frac{\partial A}{\partial t}=f_aA+\xi_a^2\frac{\partial^2A}{\partial z^2}-\delta BA^*e^{i\Delta qz}\ , \tag{6}$$

$$\frac{\partial B}{\partial t}=f_bB+\xi_b^2\frac{\partial^2B}{\partial z^2}+\delta A^2e^{-i\Delta qz}\ , \tag{7}$$

where

$$f_a=\epsilon_1-\alpha a^2-\gamma_ab^2,\quad a=|A|\ ,$$

$$f_b=\epsilon_2-\beta b^2-\gamma_ba^2,\quad b=|B|\ ,$$

and $\epsilon_{1,2}=(\text{Ta}-\text{Ta}_{1,2})/\text{Ta}_{1,2}$ are the relative distances from the onset for the Dean and Taylor modes, respectively ($\epsilon_2<0$ in the investigated region, while $\epsilon_1>0$). After linear stability calculations, the coherence lengths $\xi_a,\xi_b$ for the fundamental mode and the second harmonic mode are approximately equal, i.e., $\xi_a\simeq\xi_b$. The quantities $\alpha$, $\beta$, $\gamma_a$, and $\gamma_b$ are the coupling coefficients between the amplitude of the Dean mode and that of the Taylor mode. The sign of the hybridization terms ($\sim\delta$)

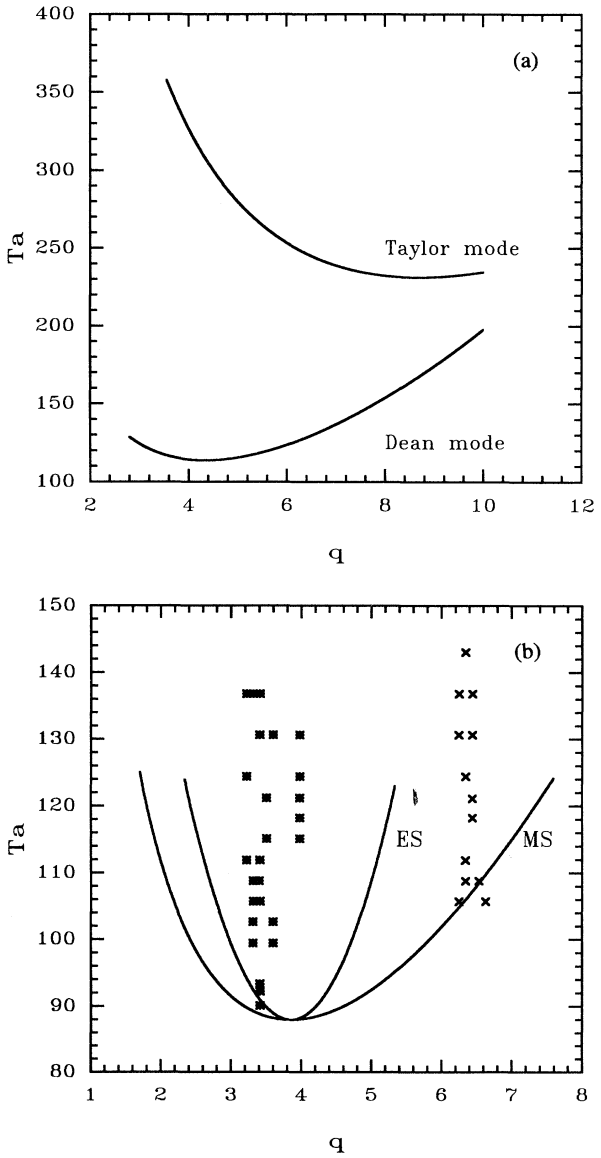


FIG. 7. Linear stability analysis results: (a) marginal stability curves for the Dean and Taylor modes for $\mu=0.714$, (b) the marginal stability curve (MS) for the Dean mode and associated Eckhaus stability curve (ES) with $\xi_0^2=0.259$ for $\mu=0.885$. The scatter points represent experimental data for $R_o=242$: * for the large rolls and × for the small rolls.

between the fundamental Dean mode and the Taylor mode is chosen in such a way that the fundamental mode tends to generate the second harmonic while the latter tends to damp the fundamental mode in the interaction process. In particular, Eq. (7) shows that the fundamental mode energy is a source of the Taylor mode which may be generated from a zero amplitude. The reduction procedure shows that the dynamics of these amplitudes is mainly governed by the dephasing between the Dean and the Taylor modes. In fact, separating the complex amplitudes into moduli and phases

$$A=ae^{i\Phi},\quad B=be^{i\Psi},$$

substituting them into the amplitude equations, and neglecting the logarithmically varying in space terms, one finds the following expressions for the amplitude moduli and phases:

$$\frac{\partial a}{\partial t}=f_a a+\xi_a^2\left[\frac{\partial^2 a}{\partial z^2}-a\left[\frac{\partial\Phi}{\partial z}\right]^2\right]-\delta ab\cos\Theta\ , \tag{8}$$

$$\frac{\partial b}{\partial t}=f_b b+\xi_a^2\left[\frac{\partial^2 b}{\partial z^2}-b\left[\frac{\partial\Psi}{\partial z}\right]^2\right]+\delta a^2\cos\Theta\ , \tag{9}$$

$$\frac{\partial\Theta}{\partial t}=\xi_a^2\frac{\partial^2\Theta}{\partial z^2}-\delta\left[2b-\frac{a^2}{b}\right]\sin\Theta+v\Delta q\ , \tag{10}$$

$$\frac{\partial\Phi}{\partial t}=\xi_a^2\frac{\partial^2\Phi}{\partial z^2}-\delta b\sin\Theta\ , \tag{11}$$

$$\frac{\partial\Psi}{\partial t}=\xi_a^2\frac{\partial^2\Psi}{\partial z^2}-\delta\frac{a^2}{b}\sin\Theta\ , \tag{12}$$

where $\Theta=\Psi-2\Phi+z\Delta q$ is the dephasing between the Dean and the Taylor modes and $v=dz/dt$ is the phase velocity. Equations (8)–(10) are very similar to those describing the second harmonic generation in a lossy nonlinear medium [15,16] in which the power can be converted from the fundamental mode into the second harmonic. The evolution equations (11) and (12) of the phases $\Phi$ and $\Psi$ give the drift frequencies of the Dean and Taylor modes. Therefore the dynamics is governed by the dephasage $\Theta$, which plays the role of the order parameter for the system [11]. Equations (8)–(12) contain the particular case of a spatially homogeneous pattern, which has been investigated recently [11]. The new term $v\Delta q$, which is due to the phase mismatching between modes, is the source term responsible for the imperfection. We consider in the following only spatially homogeneous patterns ($\partial/\partial z=0$).

### B. Perfect phase matching between modes

When there is a perfect phase matching between the Dean and the Taylor modes $\Delta q=0$, which is the case for $\mu=0.714$, and we retrieve the systems of equations investigated by other authors [11,22]. In fact, Eq. (10) can be rearranged using Eqs. (8) and (9) as follows [15]:

$$\frac{d\Theta}{dt}=H[a^2,b^2,\Theta]\sin\Theta\ , \tag{13}$$

where

$$H[a^2,b^2,\Theta]\cos\Theta=\frac{d}{dt}\ln(a^2b)+(2\alpha+\gamma_b)a^2+(\beta+2\gamma_a)b^2-(2\epsilon_1+\epsilon_2)\ . \tag{14}$$

First, we remark that the stationary solutions $a=\text{const.}\neq 0$, $b=0$, and $\Theta=0$ or $\pi$ describe the stationary axisymmetric Dean roll pattern (pure mode or mixed state) preserving reflection symmetry ($\sin\Theta=0$). In the case of a mixed state, close to the onset of the first instability, the Taylor mode will follow adiabatically the Dean mode [11]. The spontaneous breaking of the reflection symmetry occurs when the function $H[a^2,b^2,\Theta^*]=0$. The solution

$$a=a_0\neq 0,\quad b=b_0\neq 0,\quad \Theta=\Theta^*\ ,$$

is given by

$$2b_0^2=a_0^2,\quad b_0^2=\frac{(2\epsilon_1+\epsilon_2)\delta}{D}\ , \tag{15}$$

$$\cos\Theta^*=\frac{1}{\delta b}\frac{\epsilon_1(2\gamma_b+\beta)-\epsilon_2(2\alpha+\gamma_a)}{D}\ , \tag{16}$$

with the denominator $D=4\alpha+2(\gamma_b+\gamma_a)+\beta$. The solution (15) and (16) together with Eq. (11) describes a drifting cellular pattern with the drift velocity

$$v_d=\frac{1}{q}\frac{d\Phi}{dt}=\frac{\sqrt{2}}{q}\delta a\sin\Theta^*\ ,$$

where $q$ is the roll wave number. The drift velocity $v_d$ is proportional to the amplitude $a$ of the fundamental mode. Proctor and Jones [22] have shown that the traveling waves resulting from the drift instability are theoretically stable and therefore should be observable experimentally.

In fact, the observed drifting instability in our experiments is associated with a spontaneous breaking of the reflection symmetry of the stationary roll pattern, giving rise to traveling rolls inclined towards the propagation direction. At the onset of the drifting instability, the drift velocity is zero. Just above the onset of the drift transition, the rolls have a small velocity which increases with the inner cylinder Reynolds number $R_i$ as $(R_i-R_{ic})^{1/2}$ [Fig. 8(a)] which confirms that the drift instability is a supercritical transition (also no difference in onset of the drift instability was observed when ramping up and down, within the experimental limits mentioned in Sec. III A). We have observed a nonhysteretic jump at the transition.

This model also gives an estimate of the onset of the drift instability. In fact, the solutions (15) and (16) are physically acceptable if

$$0\leq[(2\alpha+\gamma_a)\epsilon_2-(\beta+2\gamma_b)\epsilon_1]^2\leq\delta^2 D(2\epsilon_1+\epsilon_2)\ . \tag{17}$$

In the parameter space of the two competing modes $(\epsilon_1,\epsilon_2)$, the equality condition gives a parabolic frontier of the drifting instability on which the phase velocity vanishes [22]. But, since in our experiments, $\epsilon_1>0$ and $\epsilon_2<0$, the weak condition $2\epsilon_1+\epsilon_2=0$ yields the approximate value of the onset $\text{Ta}^*$ of the drift instability, i.e., the value for which the second harmonic amplitude be-

comes positive definite:

$$\mathrm{Ta}^* = \frac{3\mathrm{Ta}_1\mathrm{Ta}_2}{\mathrm{Ta}_1 + 2\mathrm{Ta}_2} .$$

The criticality distance

$$\epsilon^* = \frac{\mathrm{Ta}^* - \mathrm{Ta}_1}{\mathrm{Ta}_1} = \frac{r-1}{2r+1} , \tag{18}$$

and from the critical values in Table I, one finds that the onset of the drift instability in this model is at $\epsilon^* = 0.204$, which is lower than (but comparable with) the experimental onset value $\epsilon^*_{\mathrm{expt}} = 0.280$. These values are reasonably small to make the amplitude equation model quite acceptable. The effective linear growth rate of the fundamental model $\sigma_{\mathrm{eff}} = \epsilon_1 - \gamma_a b^2 - \delta b \cos\Theta^*$ decreases as the second harmonic amplitude grows, and the growth of the second harmonic mode stabilizes the fundamental mode.

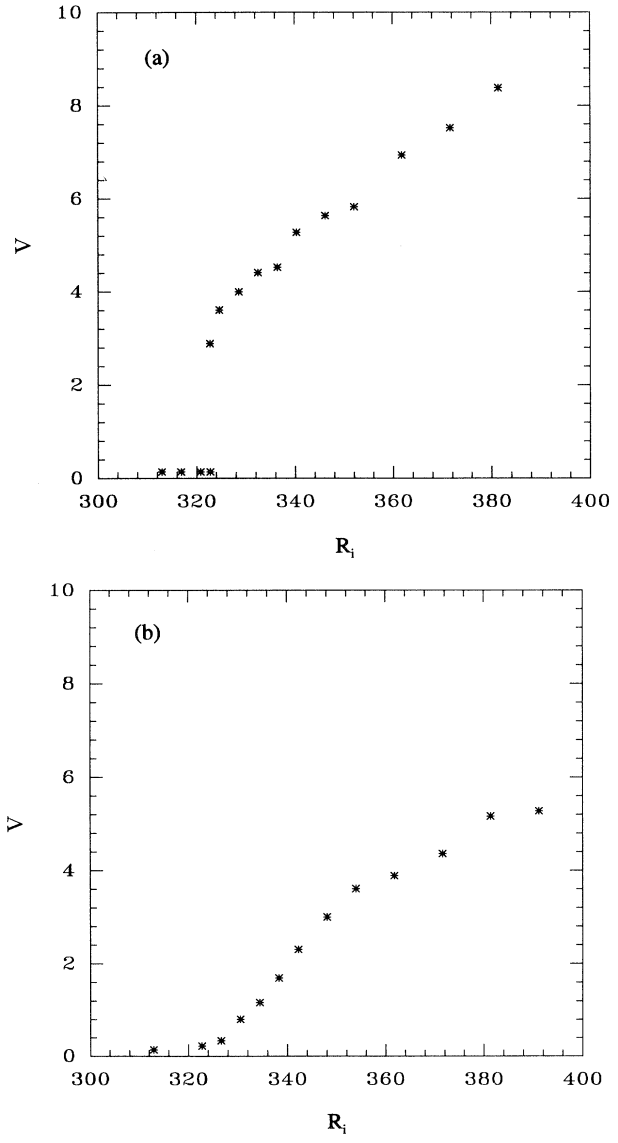


FIG. 8. Order parameter (measured drift velocity $v_d$ in units of $\nu/d$) as a function of the control parameter $R_i$: (a) for perfect phase matching ($\mu = 0.73$), (b) for imperfect phase matching ($\mu = 0.81$). There is a velocity jump at the onset of the drift instability in the case of the perfect phase matching while, for the imperfect phase matching, the drift velocity grows continuously from zero to a finite value.

### C. Imperfect phase matching

In the range of the experimental data described above, the linear stability analysis has shown that for $\mu \neq 0.714$ the competing modes have not exactly resonant wave numbers, but there is a phase mismatching between them. The interaction between the fundamental and second harmonic will be effective only if the phase matching condition is nearly satisfied, i.e., $\Delta q/q \ll 1$, which is satisfied in our experiments where $\Delta q/q \sim 0.05$. The imperfect phase matching modifies the onset neighborhood of the drift instability by introducing an imperfect bifurcation [35] on the order parameter $\Theta$. Such an imperfect bifurcation has been observed in the drift velocity measurements close to the onset of the drift instability [Fig. 8(b)]. For a steady solution $a = \text{const.} \neq 0$, $b = \text{const.} \neq 0$, $\Theta = \Theta^*$, the phase mismatch is related to the solution parameters by $v\Delta q = \delta(2b - a^2/b)\sin\Theta^*$.

### D. Halving instability

In the case of perfect phase matching, the drift frequency associated with the second harmonic mode

$$\omega_b = \frac{d\Psi}{dt} = 2\omega_a$$

can be compared with the drift frequency of the small roll pattern. The dependence of $f(R_i)$ in Fig. 4 shows also the emergence of the second harmonic frequency $f_h$ when its peak becomes larger than that of the drifting rolls. The origin of the frequency difference $\delta f = f_h - 2f_d \neq 0$ is in the imperfect phase matching but also in the phase modulations of the small drifting rolls. The existence of the interface between flow patterns of different wavelengths indicates that the transition is subcritical. The interface moves so as to eliminate the large roll state as the control parameter increases. The resulting small rolls preserve the initial wavelength, which appears as a subharmonic peak in the spatial Fourier spectrum. Moreover, the flow pattern is subject to new phase instabilities, and probably higher harmonics cannot be anymore slaved to the first two modes since they can also be excited. In fact, at their onset, the small traveling rolls are modulated in space and in time.

There exist in the literature tentative investigations [11,22] of the stability of traveling rolls resulting from the drift instability, from which standing modes are stable. In our case, the traveling rolls persist even though they are modulated with a wavelength comparable to that of the initial instability. Such modulations likely are complicated combinations of drifting and standing waves resulting from the phase instability.

The above model explains the appearance of the drifting cellular pattern, but it does not provide an explanation for the appearance of a second stable harmonic (spatial period halving). The question which arises from the

experimental data is the following: are the small rolls associated with the stability of the second harmonic with amplitude $b$ when the fundamental mode has been damped away in the interaction process or do they correspond to a different type of bifurcation? None of the stability analyses of the drifting modes done so far provide a framework for the spatial period halving, and apparently, the small rolls occur in the range of values of the control parameters where the amplitude equations are no longer valid.

## VI. CONCLUSION

The roll pattern observed in the Taylor-Dean system in the range of $R_o \in [205,250]$ exhibits an unusual sequence of transitions: the drift instability, the pattern extinction or weakening, the halving instability with coexisting rolls of different wavelengths, the onset of the small modulated roll packets, and, finally, chaotic states with a mixture of traveling and standing rolls. We have shown that, from the linear stability analysis, perfectly resonant or almost resonant modes exist in the Taylor-Dean system for $\mu \in [0.65,0.80]$. The reduction of the evolution equations of the competing modes leads to a system of equations which among others has a nontrivial solution of a drifting roll pattern. The drift instability is now understood as a result of the interaction between competing perfectly or almost resonant modes. We have used this mechanism inherent in our system to interpret experimental observations in which the order parameter is the drift velocity, which has been measured.

The simultaneous presence of large and small traveling rolls in the Taylor-Dean system is an important realization of coexisting stable time-dependent states with different spatial scales in a nonequilibrium hydrodynamics system. All observed transitions and the properties of corresponding states suggest that they originate in the interaction mechanism between the fundamental and second harmonic mode. A fully comprehensive description of the remainder of the experimental observations (halving instability, wall dynamics, stability of small modulated rolls) awaits a more comprehensive theoretical model.

## ACKNOWLEDGMENTS

The authors would like to thank L. Fourtune, J. E. Wesfried, and P. Laure for fruitful discussions on the subject and M. Degen for assistance with some of the data taking. This work was partly supported by a grant from the Direction de Recherche et Etudes Techniques (DRET) and a travel grant from NATO. I.M. would like to thank the members of the Nonlinear Dynamics Laboratory of the OSU Department of Physics for their hospitality during his visits.

[1] C. D. Andereck, S. S. Liu, and H. L. Swinney, J. Fluid Mech. **164**, 153 (1986).
[2] I. Mutabazi, J. J. Hegseth, C. D. Andereck, and J. E. Wesfreid, Phys. Rev. A **38**, 4752 (1988).
[3] P. G. Drazin and W. H. Reid, *Hydrodynamic Stability* (Cambridge University Press, Cambridge, England, 1981).
[4] I. Mutabazi, J. J. Hegseth, C. D. Andereck, and J. E. Wesfreid, Phys. Rev. Lett. **64**, 1729 (1990).
[5] A. J. Simon, J. Bechhoefer, and A. Libchaber, Phys. Rev. Lett. **61**, 2574 (1988).
[6] G. Faivre, S. de Chevigné, and P. Kurowski, Europhys. Lett. **9**, 779 (1989).
[7] M. Rabaud, S. Michalland, and Y. Couder, Phys. Rev. Lett. **64**, 184 (1990). See L. Pan and J. R. de Bruyn, Phys. Rev. E **49**, 483 (1994); **49**, 2119 (1994). The experimental results on drift instability are explained using the mode interaction suggested by Coullet, Goldstein, and Gunaratne, Phys. Rev. Lett. **63**, 184 (1989).
[8] P. Coullet, R. E. Goldstein, and G. H. Gunaratne, Phys. Rev. Lett. **63**, 184 (1989).
[9] R. E. Goldstein, G. H. Gunaratne, L. Gil, and P. Coullet, Phys. Rev. A **43**, 6700 (1991).
[10] H. G. Paap and H. Riecke, Phys. Rev. A **41**, 1943 (1990).
[11] S. Fauve, S. Douady, and O. Thual, J. Phys. (France) II **1**, 311 (1991).
[12] H. Levine, W.-J. Rappel, and H. Riecke, Phys. Rev. A **43**, 1122 (1991).
[13] B. Caroli, C. Caroli, and S. Fauve, J. Phys. (France) I **2**, 281 (1992).
[14] O. Thual and S. Fauve, J. Phys. (Paris) **49**, 1829 (1988).
[15] J. A. Armstrong, N. Bloembergen, J. Ducuing, and P. S. Pershan, Phys. Rev. **127**, 1918 (1962).
[16] L. D. Landau and E. M. Lifshitz, *Electrodynamics of Continuous Media* (Pergamon, New York, 1988).
[17] B. A. Malomed and M. I. Tribelsky, Physica D **14**, 67 (1984).
[18] R. Wiener and D. F. McAlister, Phys. Rev. Lett. **69**, 2915 (1992).
[19] H. Riecke and H.-G. Paap, Phys. Rev. A **45**, 8605 (1992).
[20] T. S. Chang and W. Sartory, J. Fluid Mech. **27**, 65 (1967).
[21] T. H. Hugues and W. H. Reid, Z. Angew. Math. Phys. **15**, 573 (1964).
[22] M. R. Proctor and C. A. Jones, J. Fluid Mech. **188**, 301 (1988).
[23] S. Rasenat, F. H. Busse, and I. Rehberg, J. Fluid Mech. **199**, 519 (1989).
[24] P. Cardin and H. C. Nataf, Europhys. Lett. **14**, 655 (1991).
[25] M. R. Proctor and P. Metzner, Eur. J. Mech. B **11**, 759 (1992).
[26] S. Chandrasekhar, *Hydrodynamic and Hydromagnetic Stability* (Oxford University Press, Clarendon, 1961). Recent development in the Taylor-Couette flow can be found in *Ordered and Turbulent Patterns in Taylor Vortex Flow,* edited by C. D. Andereck and F. Hayot (Plenum, New York, 1992).
[27] I. Mutabazi, C. Normand, H. Peerhossaini, and J. E. Wesfreid, Phys. Rev. A **39**, 452 (1989).
[28] In classical literature on the Taylor-Couette instability (e.g., [26]), the Taylor number is defined in terms of our Ta as $T=2(1-\mu)\mathrm{Ta}^2$.
[29] I. Mutabazi, Thèse de Doctorat en Physique, Université Paris 7, 1990.

[30] I. Mutabazi and C. D. Andereck, Phys. Rev. Lett. **70**, 1429 (1993).
[31] K. Park, G. L. Crawford, and R. J. Donnelly, Phys. Rev. Lett. **47**, 1448 (1981).
[32] A. Joets and R. Ribotta, in *New Trends in Nonlinear Dynamics and Pattern Forming Phenomena,* Vol. 237 of *NATO Advanced Study Institute, Series B: Physics,* edited by P. Coullet and P. Huerre (Plenum, New York, 1990), p. 125.
[33] P. Laure and I. Mutabazi, Phys. Fluids **6**, 3630 (1994).
[34] The correspondence between the parameters $(R_o, R_i)$ and $(\mu, \mathrm{Ta})$ is given by the relations $\mu = \eta R_o / R_i$ and $\mathrm{Ta} = (d/a)^{1/2} R_i$, in the small gap approximation $(\eta \simeq 1)$.
[35] P. Manneville, *Dissipative Structures and Weak Turbulence* (Academic, Boston, 1990).